Wen, S., Liu, G., Xu, F., Zhang, L., Liu, C. and Imran, M. (2022) Ergodic capacity of MIMO faster-than-nyquist transmission over triply-selective rayleigh fading channels. *IEEE Transactions on Communications*, (doi: 10.1109/TCOMM.2022.3185291)

There may be differences between this version and the published version. You are advised to consult the published version if you wish to cite from it.

http://eprints.gla.ac.uk/273125/

Deposited on 24 June 2022

Enlighten – Research publications by members of the University of Glasgow
http://eprints.gla.ac.uk

Ergodic Capacity of MIMO Faster-Than-Nyquist Transmission over Triply-Selective Rayleigh Fading Channels

Shan Wen, *Student Member, IEEE,* Guanghui Liu, *Senior Member, IEEE*, Fuchen Xu, Lei Zhang, *Senior Member, IEEE*, Chengxiang Liu, and Muhammad Ali Imran, *Senior Member, IEEE*

***Abstract*—Faster-than-Nyquist signaling (FTNS) has already been shown to increase the communication capacity on certain channels such as additive white Gaussian noise and block flat multiple-input multiple-output (MIMO) Rayleigh fading channels. The following issues, however, remain unresolved: 1) whether FTNS enables a capacity increase in generalized MIMO Rayleigh fading channels that are selective in time, frequency, and space; and 2) how channel selectivities affect the capacity and if present, the FTN capacity gain. To address the issues, this paper firstly investigates the ergodic capacity of MIMO-FTN transmission over triply-selective fading channels. We derive a low-complexity approximate capacity formula and also show how it degenerates in other channel models, such as doubly-selective single-input single-output fading channels, which can be considered as the special cases of triply-selective fading channels. The capacity evaluation results obtained under different channel conditions show that: 1) MIMO-FTN outperforms MIMO-Nyquist in terms of capacity; 2) the FTN gains are nearly consistent, while the FTN gains obtained in the frequency-selective fading channels are slightly higher than those obtained in the flat fading channels.**

***Index Terms*—Faster-than-Nyquist signaling, MIMO-FTN, triply-selective Rayleigh fading, ergodic capacity.**

I. Introduction

As a representative physical-layer non-orthogonal signaling technique, faster-than-Nyquist signaling (FTNS) is capable of increasing the communication capacity in bandwidth-limited channels [1]–[8]. Moreover, FTNS can be developed in conjunction with techniques such as non-orthogonal multiple access [9], [10], spatial multiplexing obtained by placing multiple antennas at transmitter and receiver, antenna polarization multiplexing [11], and constructive interference precoding [12], to further improve core technical indicators such as system capacity and energy efficiency. However, it is unclear how much information-theoretic capacity gain FTNS will provide when it is combined with these techniques? This paper deals with the multi-antenna FTN transmission and investigates the ergodic capacity on multi-input multi-output (MIMO) Rayleigh fading channels, followed by evaluating the FTN capacity gain. The sub-channels of the MIMO channel are triply-selective, namely frequency-selective (due to delay spread), time-selective (due to Doppler spread), and space-selective (due to angle spread at the transmitter and/or receiver).

Although studies on the capacity of FTN systems have received some attention in the past decade, the majority of them focus on single-input single-output (SISO) scenarios with additive white Gaussian channels [13]–[18] or quasi-static multi-path channels [15], [16], [19]–[21]. Specifically, in the seminal paper [13] by Rusek and Anderson, an independent and identically distributed (i.i.d.) input was assumed. Therein, it was shown that FTNS increases the capacity by utilizing the excess bandwidth of practical Nyquist pulses, e.g. raised cosine pulses. [14] formulated the capacity using the eigenvalues of FTN-induced inter-symbol interference (ISI) matrix, and the capacity expression coincides with that of [13]. By allowing correlations among input symbols, [15]–[17] studied capacity-achieving input power spectral density (PSD) under certain constraints imposed on the FTN signal's PSD. Wang [19], [20] examined the achievable information rate of block-wise FTN transmission over the multi-path channel. Moreover, time-based receive transformation was proposed such that the information rate benefits from both the increased signaling rate and the increased channel length[1]. In [18] and [21], Sugiura *et al.* derived the capacities for the eigendecomposition-precoded FTN signaling in the AWGN and frequency-selective channels, respectively. Furthermore, power allocation is optimized to maximize the capacity.

There are limited works reporting the capacity of MIMO-FTN transmission. In [1, section 4.3] and [22], block flat fading channels were considered. And the channel varies randomly from one block to another. A MIMO-FTN scheme is reported to have information rate superior to the MIMO-Nyquist counterpart for all Nyquist pulses except the sinc [1]. The conclusion suits both the cases of no channel state information (CSI) and perfect CSI at the transmitter. In [23], Wang extended the previous studies [19], [20] to the time-space MIMO systems and proposed time-space receive transformation based FTNS.

As have seen above, in the existing MIMO-FTN capacity research, the sub-channels are assumed not to have Doppler spread or spatial correlation. While these assumptions may

Shan Wen, Guanghui Liu (Corresponding author), Fuchen Xu, and Chengxiang Liu are with the School of Information and Communication Engineering, University of Electronic Science and Technology of China, Chengdu, 611731, China (e-mail: shanwen@std.uestc.edu.cn; guanghuiliu@uestc.edu.cn; {fuchenxu, cxliu}@std.uestc.edu.cn).

Lei Zhang and Muhammad Ali Imran are with the James Watt School of Engineering, University of Glasgow, Glasgow, G12 8QQ, U.K. (e-mail: {Lei.Zhang, Muhammad.Imran}@glasgow.ac.uk).

[1]It is known that channel length is determined by the ratio of the maximum delay spread to the symbol duration. FTN transmission is realized by reducing the symbol duration, leading to an increased channel length.

make the computation tractable, there are two major caveats: 1) practical (especially large-scale) MIMO channels are spatially correlated, as seen from measurement campaigns [24], [25] and physical arguments [26]; 2) in the future, communication networks will offer coverage on the ground, in the sky, and in space. Supporting mobility will lay the foundation for this vision. In fact, Wu *et al*. [27]–[29] have proposed several frequency-domain equalization algorithms to counter the combined ISI due to the FTNS and time-varying ISI channels in mobile environments.

Regarding the MIMO communications using the Nyquist signaling on triply-selective Rayleigh fading channels, Xiao *et al*. [30], [31] have developed a discrete-time channel model. They discovered that in addition to the well-known correlation in the temporal domain introduced by Doppler spread, the discrete-time channel taps exhibit correlation in the delay domain caused by the convolution of the transmit filter, the physical fading channel, and the receive filter. Furthermore, [32]–[34] demonstrated that the inter-tap correlation (ITC) can reduce ergodic capacity. As a result, the discrete-time inter-tap correlated frequency-selective fading channel has a lower ergodic capacity than the frequency flat fading channel. It should be noted that the capacity formulas in [32]–[34] were developed in the presence of white noise, whereas FTNS induces colored noise [1], [2], [6], [8].

In this paper, we firstly investigate the ergodic capacity of FTN transmission in more realistic triply-selective MIMO Rayleigh fading channels. Due to the time variations, we presume that the CSI is available at the receiver yet not at the transmitter, as in [22], [32]–[34]. We derive a low-complexity approximate capacity formula that quantifies the effects of the ITCs and colored noise on the ergodic capacity into a signal-to-noise ratio (SNR) degradation factor. Because other channel models, such as doubly-selective SISO channels, single-input and multi-output (SIMO) and multi-input and single-output (MISO) Rayleigh fading channels, can be regarded as the special cases of MIMO triply-selective fading channels, approximate capacity formulas for these channels are also presented. In all evaluated channel conditions, both the capacity results obtained using the derived formulas and the Monte-Carlo simulation (MCS) results based on the capacity definition show that FTNS enhances the ergodic capacity. It is also shown that the time and spatial selectivities have little impact on the FTN capacity gain. On the other hand, the frequency selectivity has a beneficial effect, that is, the gain obtained in the frequency-selective fading channel is slightly higher than that obtained in the flat fading channel. However, the benefit of frequency selectivity does not scale with the maximum delay spread.

The rest of this paper is organized as follows. Sec. II presents a discrete-time model for MIMO-FTN systems in triply-selective Rayleigh fading channels. In Sec. III, the ergodic capacity formulas are derived. MCS and numerical results are shown in Sec. IV to verify the derived formulas and also demonstrate the effectiveness of the FTNS. Finally, conclusions are given in Sec. V.

Notation: We use the upper-case and lower-case boldface letters to denote matrices and vectors, respectively. The transpose, Hermitian transpose and determinant of matrix $\mathbf{X}$ are denoted as $\mathbf{X}^{\mathrm{T}}$, $\mathbf{X}^{\mathrm{H}}$, and $\det(\mathbf{X})$, respectively. $\mathbb{E}\{\cdot\}$, $\mathbb{H}(\cdot)$, $(\cdot)^*$ and $\otimes$ indicate the expectation, differential entropy, conjugate and Kronecker product operators, respectively. Finally, $\mathbf{I}_N$ and $\mathbf{0}_N$ denote an identity matrix and all-zero matrix with size $N \times N$, respectively.

II. Discrete-Time Channel Model for MIMO-FTN Transmission

A. Discrete-Time Channel Model

Consider a baseband single-carrier MIMO-FTN transmission system with N transmit antennas and M receive antennas, as shown in Fig. 1. $s_n[k]$ represents the kth symbol to be transmitted from the nth transmit antenna in a signal interval of duration τT_s seconds, where T_s is the time duration of the Nyquist signaling interval and the parameter τ is called the FTN time compression factor. We assume that the same modulation pulse $p_T(t)$ is used for all transmit branches. The physical channel between the nth transmit antenna and the mth receive antenna is denoted by $c_{m,n}(t,\alpha)$, where α is the delay variable and t is the time variable. At the receiver, the analog signal at each receive branch passes through the receive filter $p_R(t)$ and the symbol-rate sampling. Let the kth sample at the mth receive antenna be denoted by $y_m[k]$, and the composite impulse response of the serial concatenation of $p_T(t)$, $c_{m,n}(t,\alpha)$ and $p_R(t)$ be denoted by $h_{m,n}(t,\alpha)$ and presented by [30], [35]

$$\begin{aligned} h_{m,n}(t,\alpha) = \int_{\alpha_1}\int_{\alpha_2} & p_R(\alpha_2)\, c_{m,n}(t-\alpha_2,\alpha_1) \\ & \times p_T(\alpha-\alpha_1-\alpha_2)\, d\alpha_1 d\alpha_2. \end{aligned} \tag{1}$$

An equivalent discrete-time model for the MIMO-FTN system is described by the input-output relation [30], [31]

$$y_m[k] = \sum_{n=1}^{N}\sum_{l} s_n[k-l]\, h_{m,n}[k,l] + z_m[k],\, k = 0,1,\ldots \tag{2}$$

where $h_{m,n}[k,l] = h_{m,n}(k\tau T_s, l\tau T_s)$ is the τT_s-sampled version of $h_{m,n}(t,\alpha)$, and $z_m[k]$ represents the noise sample and is given by

$$z_m[k] = \int_{\alpha} p_R(\alpha)\, \upsilon_m(k\tau T_s - \alpha)\, d\alpha, \tag{3}$$

where $\upsilon_m(t)$ is zero-mean additive white Gaussian noise (AWGN) with variance σ_υ^2. Also, $\upsilon_m(t)$ is independent from antenna to antenna. That is, $\mathbb{E}\{\upsilon_m(t_1)\,\upsilon_p^*(t_2)\} = \sigma_\upsilon^2 \delta(m-p)\,\delta(t_1-t_2)$, where $\delta(\cdot)$ is the Dirac delta function.

In practice, the tails of $p_T(t)$ and $p_R(t)$ are designed to decay rapidly, and $c_{m,n}(t,\alpha)$ has finite support in the α domain. Thus, the amplitudes of $h_{m,n}[k,l]$ will decrease quickly with increasing $|l|$. In this paper, we assume that $h_{m,n}[k,l] = 0$ if $l < -L_1$ or $l > L_2$, where L_1 and L_2 are nonnegative integers. $L = L_1 + L_2 + 1$ is the channel length.

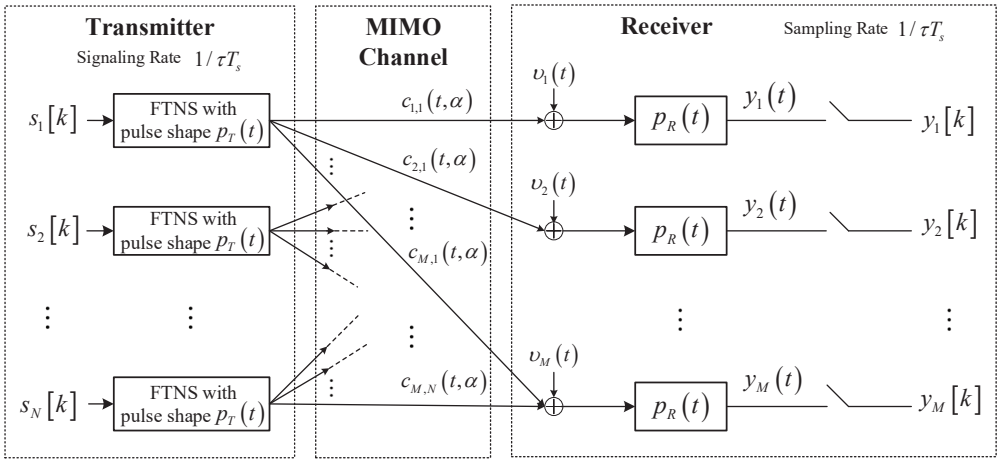

Fig. 1. Block diagram of a baseband MIMO-FTN system model.

With the channel memory truncation, a vector presentation of the received signal $y_m[k]$ of (2), representing the result of space-domain sampling, is given by

$$\begin{aligned}\mathbf{y}[k] &= [y_1[k], \ldots, y_M[k]]^{\mathrm{T}} \\ &= \sum\nolimits_{l=-L_1}^{L_2} \mathbf{H}_l[k]\,\mathbf{s}[k-l] + \mathbf{z}[k],\end{aligned} \tag{4}$$

where $\mathbf{s}[k] = [s_1[k], \ldots, s_N[k]]^{\mathrm{T}}$, $\mathbf{z}[k] = [z_1[k], \ldots, z_M[k]]^{\mathrm{T}}$, and

$$\mathbf{H}_l[k] = \begin{bmatrix} h_{1,1}[k,l] & \cdots & h_{1,N}[k,l] \\ \vdots & \ddots & \vdots \\ h_{M,1}[k,l] & \cdots & h_{M,N}[k,l] \end{bmatrix}$$

is an $M \times N$ channel matrix, comprised of the lth-tap delayed channel impulse responses at the time instant $t = k\tau T_s$.

B. Statistical Properties of the Discrete-Time Channel Model

Given that $\tau = 1$, study [31] analyzes the properties of model (4) based on the following assumptions:

1) Assumption 1: Each sub-channel $c_{m,n}(t,\alpha)$ is a wide-sense stationary uncorrelated scattering Rayleigh fading channel with zero-mean and autocorrelation given by [35]

$$\begin{aligned}&\mathbb{E}\left\{c_{m,n}(t,\alpha)\, c^*_{m,n}(t-\varepsilon,\alpha')\right\} \\ &= J_0(2\pi f_d \varepsilon) \cdot C(\alpha) \cdot \delta(\alpha-\alpha'), \forall m,n\end{aligned} \tag{5}$$

where $J_0(\cdot)$ is the zero-order Bessel function of the first kind, f_d is the maximum Doppler frequency, and $C(\alpha)$ represents the normalized channel power delay profile (PDP) with $\int_\alpha C(\alpha)\,d\alpha = 1$. For some channels that contain discrete multipath components, such as Extended Pedestrian A (EPA), Extended Vehicular A (EVA), and Extended Typical Urban (ETU) [36], an appropriate definition of $C(\alpha)$ is

$$C(\alpha) = \sum\nolimits_{p=1}^{P} \sigma_p^2 \delta(\alpha - \alpha_p), \tag{6}$$

where P is the number of resolvable multipath components, σ_p^2 and α_p are the power and propagation delay for the pth path, respectively.

2) Assumption 2: f_d is much smaller than the bandwidth of $p_R(t)$. Then $h_{m,n}(t,\alpha)$ can be approximated as [30]

$$h_{m,n}(t,\alpha) \approx \int_{\alpha'} c_{m,n}(t,\alpha')\, g_{TR}(\alpha-\alpha')\, d\alpha', \tag{7}$$

where $g_{TR}(t) = \int_\alpha p_R(\alpha)\, p_T(t-\alpha)\, d\alpha$ is the convolution of $p_T(t)$ and $p_R(t)$.

3) Assumption 3: The spatial correlations at the transmit and receive sides are separable, and

$$\begin{aligned}&\mathbb{E}\left\{c_{m,n}(t,\alpha)\, c^*_{p,q}(t-\varepsilon,\alpha')\right\} \\ &= [\mathbf{\Psi}_{T_x}]_{n,q} \cdot [\mathbf{\Psi}_{R_x}]_{m,p} \cdot J_0(2\pi f_d \varepsilon) \cdot C(\alpha) \cdot \delta(\alpha-\alpha'),\end{aligned} \tag{8}$$

where $\mathbf{\Psi}_{T_x}$ is an $N \times N$ transmit correlation coefficient matrix, and its (n,q)-entry, $[\mathbf{\Psi}_{T_x}]_{n,q}$, denotes the correlation between transmit antennas n and q with $0 \le \left|[\mathbf{\Psi}_{T_x}]_{n,q}\right| \le [\mathbf{\Psi}_{T_x}]_{n,n} = 1$; $\mathbf{\Psi}_{R_x}$ is an $M \times M$ receive correlation coefficient matrix, and its (m,p)-entry, $[\mathbf{\Psi}_{R_x}]_{m,p}$, denotes the correlation between receive antennas m and p with $0 \le \left|[\mathbf{\Psi}_{R_x}]_{m,p}\right| \le [\mathbf{\Psi}_{R_x}]_{m,m} = 1$.

Note that these assumptions are quite accurate and commonly used in the literature (e.g., [37], [38] and references therein) on MIMO Rayleigh fading channels. With such assumptions, we give two propositions to illustrate the properties of the noise vector $\mathbf{z}[k]$ and channel coefficients $h_{m,n}[k,l]$ for a general τ.

Proposition 1. *The noise vector $\mathbf{z}(k)$ is zero-mean Gaussian distributed with auto-correlation matrix $\mathbf{R}_{\mathbf{zz}}(k_1-k_2)$ given by*

$$\mathbf{R}_{\mathbf{zz}}(k_1-k_2) = \sigma_\upsilon^2 g_\tau[k_1-k_2]\,\mathbf{I}_M, \tag{9}$$

where

$$g_\tau[k] = \int p_R(t)\, p_R^*(t-k\tau T_s)\, dt. \tag{10}$$

Proposition 2. *The correlation function between the channel coefficients $h_{m,n}[k_1,l_1]$ and $h_{p,q}[k_2,l_2]$ is given by*

$$\begin{aligned}&\mathbb{E}\left\{h_{m,n}[k_1,l_1]\, h^*_{p,q}[k_2,l_2]\right\} \\ &= [\mathbf{\Psi}_{T_x}]_{n,q} [\mathbf{\Psi}_{R_x}]_{m,p} J_0(2\pi f_d (k_1-k_2)\tau T_s)\, c[l_1,l_2],\end{aligned} \tag{11}$$

where $c[l_1,l_2]$, denoting the ITC coefficient, is given by

$$c[l_1,l_2]=\begin{cases}\int_{\alpha} g_{TR}(l_1\tau T_s-\alpha)\, g_{TR}^{*}(l_2\tau T_s-\alpha)\, C(\alpha)\, d\alpha, \\ \qquad\qquad \textit{if } C(\alpha) \textit{ is continuous} \\ \sum_{p=1}^{P}\sigma_p^2 g_{TR}(l_1\tau T_s-\alpha_p)\, g_{TR}^{*}(l_2\tau T_s-\alpha_p), \\ \qquad\qquad \textit{if } C(\alpha) \textit{ is given by (6)}\end{cases} \tag{12}$$

(11) shows that the ITC renders the channel coefficients from different sub-channels with different delays statistically correlated. We are interested in which cases the ITCs vanish, i.e., $c[l_1,l_2]=\delta[l_1]\cdot\delta[l_2]$. For the Nyquist signaling, where $g_{TR}(lT_s)=1$ for $l=0$ and $g_{TR}(lT_s)=0$ for $l\neq 0$, according to (12), there exist two cases. One is that the fading channel is frequency non-selective, with $C(\alpha)=\delta(\alpha)$. In the second case, $C(\alpha)$ is given by (6), and α_p is an integer multiple of T_s for all p. In other circumstances, the frequency-selective channels lead to the ITC for the Nyquist signaling. Since $g_{TR}(l\tau T_s)\neq 0$ for $l\neq 0$, the ITC always exists for the FTNS, regardless of channel frequency selectivity.

C. Generation of Coefficients $h_{m,n}[k,l]$

This section introduces an approach outlined in [31] for generating the channel coefficients $\{h_{m,n}[k,l]\}$. Note that (4) involves MNL channel coefficients at time k. It is convenient to arrange these coefficients in an MNL-element vector as follows

$$\begin{aligned}\mathbf{h}_{\text{vec}}[k]=[&\mathbf{h}_{1,1}[k],\ldots\mathbf{h}_{1,N}[k],\mathbf{h}_{2,1}[k],\ldots,\\ &\mathbf{h}_{M,1}[k],\ldots,\mathbf{h}_{M,N}[k]]^{\mathrm{T}},\end{aligned} \tag{13}$$

where $\mathbf{h}_{m,n}[k]\triangleq[h_{m,n}[k,-L_1],\ldots h_{m,n}[k,L_2]]\in\mathbb{C}^{1\times L}$. The theorem 2 in [31] states that $\mathbf{h}_{\text{vec}}[k]$ can be generated by

$$\mathbf{h}_{\text{vec}}[k]=\left(\mathbf{\Psi}_{R_x}^{1/2}\otimes\mathbf{\Psi}_{T_x}^{1/2}\otimes\mathbf{C}_{\text{ITC}}^{1/2}\right)\mathbf{\Phi}[k], \tag{14}$$

where $\mathbf{C}_{\text{ITC}}\in\mathbb{C}^{L\times L}$ is the covariance matrix of $\mathbf{h}_{m,n}[k]$ with elements $c[l_1,l_2], -L_1\leqslant l_1,l_2\leqslant L_2$; $\mathbf{\Phi}[k]\in\mathbb{C}^{MNL\times 1}$ consists of elements that are uncorrelated Rayleigh fading, and $\mathbb{E}\left\{\mathbf{\Phi}[k_1]\,\mathbf{\Phi}^{\mathrm{H}}[k_2]\right\}=J_0(2\pi f_d(k_1-k_2)\tau T_s)\,\mathbf{I}_{MNL}$.

III. Ergodic Capacity Computation

In this section, we first define the ergodic capacity for a MIMO-FTN system experiencing triply-selective fading. Afterward, the simplified formula is derived to facilitate the calculation. Capacity formulas are also derived for the SISO, SIMO, and MISO cases.

A. Definition of Ergodic Capacity

Due to the ISI, the calculation of ergodic capacity entails observations $\mathbf{Y}_K=\left[\mathbf{y}^{\mathrm{T}}[k],\ldots,\ \mathbf{y}^{\mathrm{T}}[k+K-1]\right]^{\mathrm{T}}\in\mathbb{C}^{KM\times 1}$, where $K\gg L$. By defining a $KM\times(K+L-1)N$ space-time channel matrix

$$\mathcal{H}=\begin{bmatrix}\mathbf{H}_{L_2}[k] & \cdots & \mathbf{H}_{-L_1}[k] & \mathbf{0}\\ \vdots & \ddots & \ddots & \vdots\\ \mathbf{0} & \mathbf{H}_{L_2}[k+K-1] & \cdots & \mathbf{H}_{-L_1}[k+K-1]\end{bmatrix},$$

it is possible to express $\mathbf{Y}_K$ as

$$\mathbf{Y}_K=\mathcal{H}\mathbf{S}_{K+L-1}+\mathbf{Z}_K, \tag{15}$$

where the vectors $\mathbf{S}_{K+L-1}=\left[\mathbf{s}^{\mathrm{T}}[k-L_2],\ldots,\mathbf{s}^{\mathrm{T}}[k+K-1+L_1]\right]^{\mathrm{T}}\in\mathbb{C}^{(K+L-1)N\times 1}$, $\mathbf{Z}_K=\left[\mathbf{z}^{\mathrm{T}}[k],\ldots,\mathbf{z}^{\mathrm{T}}[k+K-1]\right]^{\mathrm{T}}\in\mathbb{C}^{KM\times 1}$ comprise all the transmitted symbols and noise samples related to $\mathbf{Y}_K$.

With proposition 1, it can be easily shown that the noise vector $\mathbf{Z}_K$ is zero-mean Gaussian distributed with auto-correlation matrix $\mathbf{R}_{\mathbf{ZZ}}$ given by

$$\mathbf{R}_{\mathbf{ZZ}}=\sigma_v^2\mathbf{G}_\tau\otimes\mathbf{I}_M=\sigma_v^2\tilde{\mathbf{R}}_{\mathbf{ZZ}}, \tag{16}$$

where $\mathbf{G}_\tau$ is a $K\times K$ toeplitz matrix

$$\mathbf{G}_\tau=\begin{bmatrix}g_\tau[0] & g_\tau[-1] & \cdots & g_\tau[1-K]\\ g_\tau[1] & g_\tau[0] & \ddots & \vdots\\ \vdots & \ddots & \ddots & g_\tau[-1]\\ g_\tau[K-1] & \cdots & g_\tau[1] & g_\tau[0]\end{bmatrix}.$$

Note that for a finite K, $\mathbf{G}_\tau$ is positive definite, irrespective of τ [8], [14], [21]. However, as K goes to infinity, the positive-definiteness of $\mathbf{G}_\tau$ depends on τ for a given fixed receive filter $p_R(t)$ [21]. For example, when a root raised cosine (RRC) filter with roll-off factor β is used, $\tau\geqslant 1/(1+\beta)$ should be satisfied [8], [11], [14], [21].

In this paper, we assume that the channel matrix $\mathcal{H}$ is known by the receiver precisely, but the transmitter cannot acquire the knowledge of $\mathcal{H}$. Moreover, the transmitter does not have access to the spatial correlation matrices although we treat $\mathbf{\Psi}_{T_x}$ and $\mathbf{\Psi}_{R_x}$ as deterministic. The resulting capacity-achieving input vector is independent complex Gaussian with equal power on each of the antennas. Denoting by P the total power over the N antennas and keeping in mind that the average transmit power of the FTN signal is $\sigma_s^2/(\tau T_s)$ [1, eq. (3.8)] as $\mathbb{E}\{s_n[k]\,s_n^*[k-k_0]\}=\sigma_s^2\delta[k_0]$, then the covariance matrix of the input vector is

$$\mathbf{R}_{\mathbf{SS}}=\frac{P\tau T_s}{N}\mathbf{I}_{(K+L-1)N}. \tag{17}$$

For a deterministic $\mathcal{H}$, the mutual information per input symbol is computed as (18), shown at the top of next page. To obtain (18c), we have assumed that the value of τ is selected in such a way that $\mathbf{G}_\tau$ is positive definite and then $\tilde{\mathbf{R}}_{\mathbf{ZZ}}$ is invertible. In the last step we have applied the decomposition $\tilde{\mathbf{R}}_{\mathbf{ZZ}}^{-1}=\tilde{\mathbf{R}}_{\mathbf{ZZ}}^{-1/2}\left(\tilde{\mathbf{R}}_{\mathbf{ZZ}}^{-1/2}\right)^{\mathrm{H}}$ and the identity $\det(\mathbf{I}+\mathbf{AB})=\det(\mathbf{I}+\mathbf{BA})$, and introduced three new variables: $\text{SNR}=PT_s/\sigma_v^2$; the normalized SNR $\gamma=\text{SNR}/N$; $\tilde{\mathcal{H}}=\tilde{\mathbf{R}}_{\mathbf{ZZ}}^{-1/2}\mathcal{H}$. By normalizing $\mathcal{I}_K(\mathcal{H})$ with $1/\tau$ and taking expectation over the statistics of the random matrix $\mathcal{H}$, the ergodic capacity of MIMO-FTN system is found as follows

$$\mathcal{C}_{MIMO}^{av}=\frac{1}{\tau}\mathbb{E}_{\mathcal{H}}\{\mathcal{I}_K(\mathcal{H})\}\ \text{bits}/T_s\ \text{seconds}. \tag{19}$$

It should be noted that pioneering studies [32]–[34] considered a channel model (15) with white noise, i.e., $\tilde{\mathbf{R}}_{\mathbf{ZZ}}=\mathbf{I}_{KM}$. Here we modify the definition to handle the scenario with colored noise caused by the FTNS.

$$\mathcal{I}_K(\mathcal{H}) = \lim_{K\to\infty} \frac{1}{K}\left[\mathbb{H}(\mathbf{Y}_K) - \mathbb{H}(\mathbf{Z}_K)\right] \tag{18a}$$

$$= \lim_{K\to\infty} \frac{1}{K}\left\{\log_2\det\left[\frac{P\tau T_s}{N}\mathcal{H}\mathcal{H}^{\mathrm{H}} + \sigma_v^2\tilde{\mathbf{R}}_{\mathbf{ZZ}}\right] - \log_2\det\left[\sigma_v^2\tilde{\mathbf{R}}_{\mathbf{ZZ}}\right]\right\} \tag{18b}$$

$$= \lim_{K\to\infty} \frac{1}{K}\left\{\log_2\det\left[\frac{P\tau T_s}{N\sigma_v^2}\tilde{\mathbf{R}}_{\mathbf{ZZ}}^{-1}\mathcal{H}\mathcal{H}^{\mathrm{H}} + \mathbf{I}_{KM}\right]\right\} \tag{18c}$$

$$= \lim_{K\to\infty} \frac{1}{K}\left\{\log_2\det\left[\tau\gamma\widetilde{\mathcal{H}}\widetilde{\mathcal{H}}^{\mathrm{H}} + \mathbf{I}_{KM}\right]\right\} \qquad \text{bits/channel use.} \tag{18d}$$

Remark 1. Theoretically, the computation based on the capacity definitions (18) and (19) is mathematically unmanageable because of the infinite sized channel matrix $\tilde{\mathcal{H}}$. In spite of this, it is possible to obtain an approximate value of $\mathcal{C}_{MIMO}^{av}$ by using MCS techniques. That is, set K with a large number, e.g. 1000. Then, generate many realizations of the channel matrix $\mathcal{H}$, compute the channel capacity for each realization and take their average. This is guaranteed to converge by the law of large numbers. Nevertheless, the MCS techniques have prohibitively high complexity. To illustrate, consider $M = 4$, $K = 1000$, and 10^6 channel realizations. Then the complexity of capacity computation is about $\mathcal{O}\left(6.4\times10^{16}\right)$, provided that the computational complexity of $\det\left[\tau\gamma\tilde{\mathcal{H}}\tilde{\mathcal{H}}^{\mathrm{H}} + \mathbf{I}_{KM}\right]$ is about $\mathcal{O}\left(K^3M^3\right)$.

In the following subsections, we derive the simplified capacity formulas by exploiting the decomposition property (11) and using mean-value theorem for integrals. We start with the SISO case for better clarity.

B. Doubly-Selective SISO Rayleigh Fading Channels

Proposition 3. *The ergodic capacity for SISO-FTN system under a doubly-selective Rayleigh fading channel is given by*

$$\mathcal{C}_{SISO}^{av} = \frac{1}{\tau}\int_0^\infty\left\{\frac{1}{2\pi}\int_0^{2\pi}\log_2\left(1+\tau\gamma\lambda\frac{f(\omega)}{g(\omega)}\right)d\omega\right\}e^{-\lambda}d\lambda, \tag{20}$$

where $g(\omega) = \sum_k g_\tau[k]\,e^{-j\omega k}$ *and*

$$f(\omega) = \sum_{l=-L_1}^{L_2} c[l,l] + 2\sum_{k=1}^{L-1}\left(\sum_{l=-L_1}^{L_2-k} c[l,l+k]\right)\cos(k\omega). \tag{21}$$

Furthermore, $\mathcal{C}_{SISO}^{av}$ *can be accurately approximated*[2] *by*

$$\mathcal{C}_{SISO}^{av} = \frac{1}{\tau}\int_0^\infty \log_2\left(1+\gamma\cdot\gamma_{\mathrm{SNR}}\cdot\lambda\right)e^{-\lambda}d\lambda, \tag{22}$$

where γ_{SNR} *describes the SNR degradation due to the ITCs and the FTNS, defined as*

$$\gamma_{\mathrm{SNR}} = \left(2^{C_\gamma}-1\right)/\gamma \tag{23}$$

with

$$C_\gamma = \frac{1}{2\pi}\int_0^{2\pi}\log_2\left(1+\tau\gamma\frac{f(\omega)}{g(\omega)}\right)d\omega. \tag{24}$$

[2]Due to the lack of a two-dimensional mean-value theorem for the double integrals, despite the same numerical integration results of (20) and (22), we follow [33], [34] and make a conservative statement.

By (23), (22) can also be expressed as

$$\mathcal{C}_{SISO}^{av} = \frac{1}{\tau}\int_0^\infty \log_2\left(1+\left(2^{C_\gamma}-1\right)\lambda\right)e^{-\lambda}d\lambda. \tag{25}$$

Proof. Please see Appendix A. □

The proof exploits the fact that for ergodic fading channels, the time variation does not affect the ergodic capacity [33], [34]. The MCS results obtained based on (19) presented in Sec. IV of this paper, corresponding to three Doppler shifts, support this claim. Recall that the ITC occurs because of frequency selectivity and the FTNS. Also, correlation exists between noise components. We introduce quantity γ_{SNR} or C_γ to quantify the combined impacts of these two types of correlation on ergodic capacity. Prior to a further discussion about γ_{SNR}, we first determine the capacity of SISO-FTN transmission over the AWGN channel.

Corollary 1. *Consider the AWGN channel and* $p_R(t)$ *is matched to* $p_T(t)$*, i.e.* $p_R(t) = p_T^*(-t)$*. The capacity of SISO-FTN transmission in bits/s is*

$$\mathcal{C}_{SISO-FTN}^{AWGN} = 2\int_0^{1/2\tau T_s}\log_2\left(1+\frac{P}{\sigma_v^2}P_R^{fo}(f)\right)df, \tag{26}$$

where $P_R^{fo}(f) = \sum_k\left|P_R\left(f+\frac{k}{\tau T_s}\right)\right|^2, |f| \leqslant 1/2\tau T_s$*, is referred to the folded spectrum of* $|P_R(f)|^2$*, and* $P_R(f)$ *is the frequency response of* $p_R(t)$*. Note that (26) is the exact capacity expression that was first rigorously derived by Rusek in [1, eq. (3.19)].*

If $p_R(t)$ *is also* T_s*-orthogonal,*

$$\gamma_{\mathrm{SNR}} \leqslant 1, \tag{27}$$

where equality holds if and only $\tau = 1$.

Proof. Please see Appendix B. □

From the discussion following (12), we recall that the ITC does not exist for the communications using Nyquist signaling and experiencing frequency flat fading. In such a case, corollary 1 shows that $\gamma_{\mathrm{SNR}} = 1$, i.e., there is no SNR loss. Because FTNS always results in the ITCs, even when the fading channels are frequency flat, corollary 1 also states that $\gamma_{\mathrm{SNR}} < 1$ in the FTN case. In [33], [34], where Nyquist signaling is considered and the ITCs are induced by channel frequency selectivity, it is found that $\gamma_{\mathrm{SNR}} < 1$. Furthermore, γ_{SNR} usually decreases if the ITC increases. The ITC is projected to become stronger when considering both the FTNS and frequency-selective fading channel. Thus, the

effect of frequency-selective fading on the FTN transmission is to reduce γ_{SNR} further.

As an example, plots of γ_{SNR} versus τ for different values of SNR and different channel PDPs are shown in Fig. 2. The RRC pulse with roll-off factor $\beta = 0.22$ is used as the transmit and receive filters. The signaling rate in Nyquist signaling is 3.84 MHz with a symbol period $T_s = 260.42$ ns[3]. The channel coefficients $h_{m,n}[k,l]$ are generated using the approach presented in Sec. II-C. To guarantee that $\mathbf{G}_\tau$ is positive definite, only the values of τ in the interval $[1/(1+\beta), 1]$ are assessed. Fig. 2 illustrates that

- The FTN transmission has a smaller γ_{SNR} in contrast to the Nyquist counterpart for both the frequency-selective and -flat fading channels, as expected.
- When the ITC arises, i.e., $\gamma_{\text{SNR}} < 1$, γ_{SNR} decreases as SNR increases.
- In the FTN case, γ_{SNR} decreases as τ decreases.
- For low to moderate FTN-ISI levels that correspond to relatively large values of τ (e.g., 0.95), γ_{SNR} varies, depending on the channel PDP. When the FTN-ISI is serious or τ approaches $1/(1+\beta)$, γ_{SNR} nearly keeps constant, regardless of the channel PDP. This is due to the fact that the FTN-ISI is now considerably greater than the channel-induced ISI, and the ITCs are primarily attributable to the FTNS.

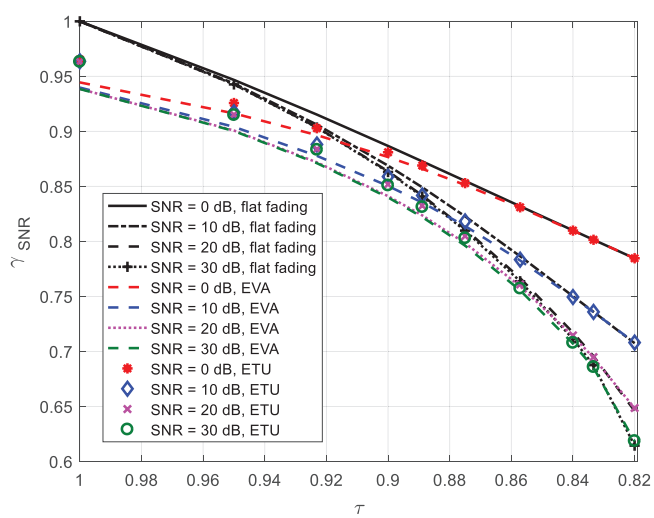

Fig. 2. The SNR degradation due to the ITC and FTNS.

Based on the relationship between γ_{SNR} and τ, we argue that there is a tradeoff between mutual information and signaling rate for the FTN transmission. By comparing (22) and (19), we observe that the integral $\int_0^\infty \log_2(1+\gamma\cdot\gamma_{\text{SNR}}\cdot\lambda)\, e^{-\lambda} d\lambda$ approximately equals the ergodic mutual information $\mathbb{E}_{\mathcal{H}}\{\mathcal{I}_K(\mathcal{H})\}$. Since γ_{SNR} decreases monotonically as τ decreases, the FTN system with a smaller τ (or a higher signaling rate) suffers from a higher mutual information loss. Nevertheless, looking at the term $1/\tau$ that appears in the expression for $\mathcal{C}^{av}_{SISO}$, thanks to the increased signaling rate, the capacity loss caused by a degradation in mutual information can be compensated to some extent. The philosophy of FTNS is to achieve a favorable tradeoff between mutual information and signaling rate.

[3]The RRC filter settings are adopted in the universal mobile telecommunications systems [39].

C. Triply-Selective Rayleigh Fading Channels

Now, we establish a simplified formula for the MIMO-FTN, analogous to proposition 3.

Proposition 4. *For triply-selective MIMO Rayleigh fading channel, the ergodic capacity is given by*

$$\mathcal{C}^{av}_{MIMO} = \frac{1}{\tau}\mathbb{E}_{\mathbf{H}_W}\left\{\frac{1}{2\pi}\int_0^{2\pi}\log_2\det\left(\mathbf{I}_M + \tau\gamma\frac{f(\omega)\,\mathbf{\Psi}_{R_x}\mathbf{H}_W\mathbf{\Psi}_{T_x}\mathbf{H}_W^H}{g(\omega)}\right)d\omega\right\} \tag{28}$$

and can be accurately approximated by

$$\mathcal{C}^{av}_{MIMO} = \frac{1}{\tau}\mathbb{E}_{\mathbf{H}_W}\left\{\log_2\det\left(\mathbf{I}_M + \left(2^{C_\gamma}-1\right)\mathbf{\Psi}_{R_x}\mathbf{H}_W\mathbf{\Psi}_{T_x}\mathbf{H}_W^H\right)\right\}, \tag{29}$$

where $\mathbf{H}_W$ is an $M\times N$ matrix with all elements being i.i.d. zero-mean circularly symmetric complex Gaussian (ZMCSCG) random variables, and C_γ is defined as (24)[4].

Proof. Please see Appendix C. □

Remark 2. In proposition 4, a significant step towards simplifying the capacity calculation is made by reducing the infinite-sized random matrix $\tilde{\mathcal{H}}$ to a finite and much smaller $M\times N$ matrix $\mathbf{H}_W$. When using MCS techniques to calculate (29) and (19), with the complexity analysis in *Remark* 1, we can conclude that the former has a computational complexity 10^9 times (if $K = 1000$) smaller than the latter.

Remark 3. Equations (12), (21) and (24) show that C_γ is independent of the spatial correlations. Since C_γ includes the effect of frequency selectivity on the capacity, from (29), we conclude that the effects of frequency selectivity and spatial selectivity on the capacity are separable. In [38], Chuah *et al.* analyzed the asymptotic behavior of mutual information of multi-antenna systems under equal-power allocation. The mutual information is given by $I^\circ = \log_2\det\left(\mathbf{I}_M + \gamma\mathbf{\Psi}_{R_x}\mathbf{H}_W\mathbf{\Psi}_{T_x}\mathbf{H}_W^{\text{H}}\right)$ for each realization of $\mathbf{H}_W$. Chuah *et al.* pointed out that 1) at low SNR, I° depends only on γ and spatial correlation has no effect on I°; 2) at high SNR, the spatial correlation reduces I° and the stronger the correlation, the greater the loss. By comparing I° with $\mathcal{C}^{av}_{MIMO}$, we see similar conclusions can be drawn for $\mathcal{C}^{av}_{MIMO}$.

From (29), we obtain three corollaries describing the capacity formulas for SIMO and MISO channels and spatial uncorrelated MIMO channels.

Corollary 2. *For triply-selective SIMO and MISO Rayleigh fading channels, the ergodic capacities $\mathcal{C}^{av}_{SIMO}$ and $\mathcal{C}^{av}_{MISO}$ can be accurately approximated with a unified form*

$$\frac{1}{\tau}\int_0^\infty \log_2\left(1+\left(2^{C_\gamma}-1\right)\lambda\right)p_\lambda(\lambda)\,d\lambda, \tag{30}$$

[4]We remind that for a given SNR, the SISO and MIMO systems have different values of γ and C_γ.

where in the SIMO case, $p_\lambda(\lambda) = \sum_{k=1}^{M} \vartheta_k \varsigma_k^{-1} e^{-\lambda/\varsigma_k}$ *with* $\vartheta_k = \prod_{i=1, i\neq k}^{M} \frac{\varsigma_k}{\varsigma_k - \varsigma_i}$ *and* ς_k *being the kth eigenvalue of* $\mathbf{\Psi}_{R_x}$*; in the MISO case,* $p_\lambda(\lambda) = \sum_{k=1}^{N} \vartheta_k \varsigma_k^{-1} e^{-\lambda/\varsigma_k}$ *with* $\vartheta_k = \prod_{i=1, i\neq k}^{N} \frac{\varsigma_k}{\varsigma_k - \varsigma_i}$ *being the kth eigenvalue of* $\mathbf{\Psi}_{T_x}$.

The readers are referred to [34] for the proof.

Corollary 3. *For a time-varying, frequency-selective, and spatially uncorrelated (i.e.* $\mathbf{\Psi}_{T_x} = \mathbf{I}_N$ *and* $\mathbf{\Psi}_{R_x} = \mathbf{I}_M$*) MIMO Rayleigh fading channel, the ergodic capacity of the MIMO-FTN system can be accurately approximated by*

$$\mathcal{C}_{MIMO}^{av} = \frac{1}{\tau} \int_0^\infty \log_2\left(1 + \left(2^{C_\gamma} - 1\right)\lambda\right) V(\lambda)\, d\lambda, \quad (31)$$

where

$$V(\lambda) = \sum_{k=0}^{m_0-1} \frac{k!}{(k+n_0-m_0)!} \left[L_k^{n_0-m_0}(\lambda)\right]^2 \lambda^{n_0-m_0} e^{-\lambda} \quad (32)$$

with $m_0 = \min(M, N)$*,* $n_0 = \max(M, N)$*, and* $L_k^l(\cdot)$ *being the associated Laguerre polynomial of order k [40].*

Proof. Please see Appendix C. □

By taking either N or M equal to 1, we can deduce the ergodic formulas for the spatial uncorrelated SIMO and MISO scenarios.

Corollary 4. *For doubly-selective SIMO and MISO Rayleigh fading channels, if the sub-channels are spatially uncorrelated, i.e.* $\mathbf{\Psi}_{R_x} = \mathbf{I}_M$ *in the SIMO case and* $\mathbf{\Psi}_{T_x} = \mathbf{I}_N$ *in the MISO case, the ergodic capacities can be accurately approximated by*

$$\mathcal{C}_{SIMO}^{av} = \frac{1}{\tau(M-1)!} \int_0^\infty \log_2\left(1 + \left(2^{C_\gamma} - 1\right)\lambda\right) \times \lambda^{M-1} e^{-\lambda} d\lambda, \quad (33)$$

$$C_{MISO}^{av} = \frac{1}{\tau(N-1)!} \int_0^\infty \log_2\left(1 + \left(2^{C_\gamma} - 1\right)\lambda\right) \times \lambda^{N-1} e^{-\lambda} d\lambda. \quad (34)$$

Note that the channels in the above propositions and corollaries are assumed to be frequency-selective. Actually, the derived formulas suit for flat fading cases just by setting the channel PDP $C(\alpha) = \delta(\alpha)$.

IV. Capacity Evaluation

In this section, we evaluate the ergodic capacities of FTN systems in a triply (doubly) selective Rayleigh fading environment, as well as validate the capacity formulas derived in Sec. III-B and Sec. III-C. We treat four types of antenna configuration: SISO, 1×4 (SIMO), 4×1 (MISO), 4×4 (MIMO). The RRC filter is used as the transmit and receive filters. The signaling rate in Nyquist signaling is 3.84 MHz with a symbol period $T_s = 260.42$ ns. We consider $\beta = 0.22$ and the EVA channel profile, unless specified otherwise.

Fig. 3 illustrates the MCS results of $\mathcal{C}_{SISO}^{av}$ for $\tau = 1$ and 5/6, with the Doppler shift f_d as a parameter. It is clear that the time variations have no effect on the ergodic capacity. Thus,

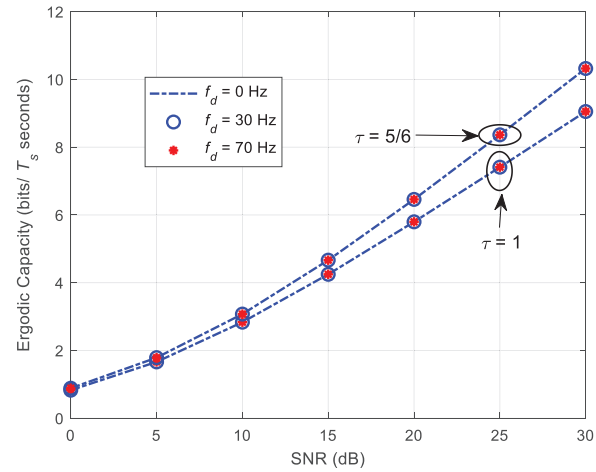

Fig. 3. Plots of $\mathcal{C}_{SISO}^{av}$ for $\tau = 1$, 5/6 and different Doppler shifts.

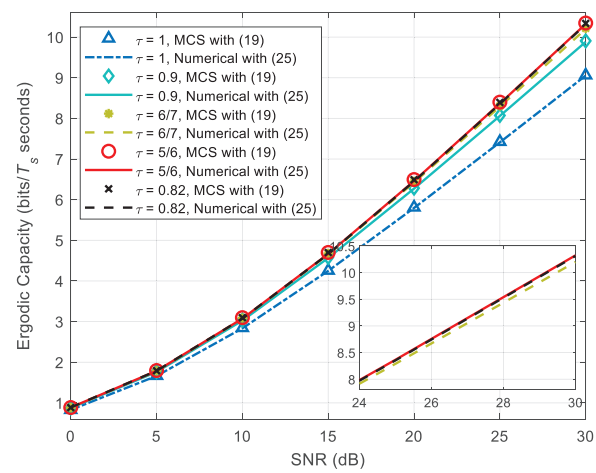

Fig. 4. Ergodic capacity of SISO-FTN system.

in the following evaluation, a fixed Doppler shift f_d of 70 Hz is selected.

Plots of $\mathcal{C}_{SISO}^{av}$ as a function SNR for different values of τ are given in Fig. 4. We note from Fig. 4 that: (*i*) the results obtained through MCS with (19) are in good agreement with those evaluated numerically from (25); (*ii*) FTNS benefits for the ergodic capacity, and the capacity gain is more noticeable at high SNR than at low SNR; (*iii*) $\mathcal{C}_{SISO}^{av}$ reaches its maximum at around $\tau = 5/6$ (in this example). It is worth noting that the capacity of an FTN system that transmits over the AWGN channel has a maximum at $\tau = 1/(1+\beta) \approx 0.8196$ [1], [8], [13]. The higher value of the capacity-optimal τ (denoted by τ°) for the FTN transmission over doubly-selective fading channels is owing to the fact that γ_{SNR} decreases with decreasing τ, as illustrated in Fig. 2. A smaller γ_{SNR} results in less mutual information. When τ is less than 5/6, the degradation of mutual information cancels out the increased signaling rate. The values of τ° as well as $1/(1+\beta)$ are given in Tab. I when β takes other values in the range of $(0, 1]$. It is seen that τ° is slightly larger than $1/(1+\beta)$.

Let us use η to denote the spectral efficiency (SE) of FTN

TABLE I
τ° VERSUS β. HERE THE EVA CHANNEL PROFILE IS CHOSEN.

β	0.1	0.2	0.3	0.4	0.5	0.6	0.7	0.8	0.9	1
τ°	0.9167	0.84	0.7857	0.7255	0.68	0.64	0.6	0.58	0.54	0.5152
$1/(1+\beta)$	0.9091	0.8333	0.7692	0.7143	0.6667	0.625	0.5882	0.5556	0.5263	0.5

signaling with the RRC pulses. In line with previous works [8], [13], η is defined as

$$\eta = \mathcal{C}_{SISO}^{av} / (1+\beta), \frac{\text{bps}}{\text{Hz}} \tag{35}$$

Obviously, the maximum value of η, denoted by $\eta_{\max}$, appears at $\tau = \tau^{\circ}$. Plots of $\eta_{\max}$ for $\beta = 0.1$, 0.4, 0.7 and 1 are shown in Fig. 5. The SE performance of the Nyquist signaling schemes employing the same RRC shaping filter and a sinc filter is also provided for comparison purposes. We observe that the FTN signaling scheme surpasses the Nyquist counterpart given $\beta > 0$. Moreover, the performance advantage is substantial especially for high SNRs and moderate to large β. Fig. 5 also shows that with increasing β, the achievable SE for both the FTN and Nyquist signaling schemes falls. Similar observations have been found in the AWGN channel [8].

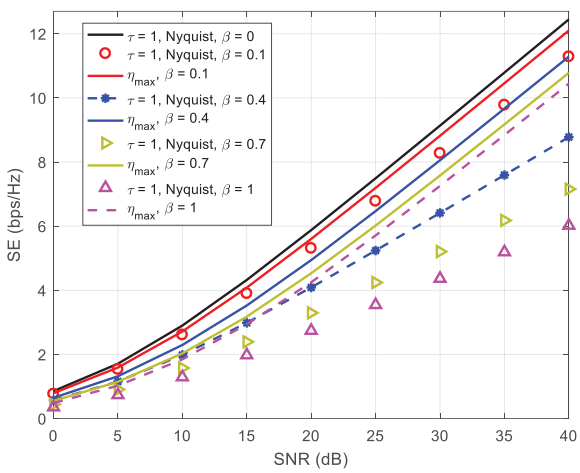

Fig. 5. Comparison of achievable SE for FTNS and Nyquist signaling in the EVA channel.

We are now in a position to treat the multi-antenna cases. For brevity, we shall limit our evaluation to $\tau = 5/6$. Fig. 6 shows the capacity results of 4×4 MIMO-FTN systems with the transmit and the receive correlation matrices being

$$\mathbf{\Psi}_{T_x} = \mathbf{\Psi}_{R_x} = \begin{bmatrix} 1 & \rho^{1/9} & \rho^{4/9} & \rho \\ \rho^{1/9} & 1 & \rho^{1/9} & \rho^{4/9} \\ \rho^{4/9} & \rho^{1/9} & 1 & \rho^{1/9} \\ \rho & \rho^{4/9} & \rho^{1/9} & 1 \end{bmatrix}$$

and the transmit correlation coefficient $\rho_{\text{Tx}} \in \{0, 0.3, 0.9\}$, the receive correlation coefficient $\rho_{\text{Rx}} \in \{0, 0.9\}$. Note that the spatial-correlation matrices are defined in the LTE specification [36] for a 4×4 antenna configuration. Moreover, 0, 0.3, and 0.9 correspond to low (actually no correlation), medium, and high correlation levels, respectively. The capacities of the 4×1 (MISO) and 1×4 (SIMO) channels are shown in Fig. 7

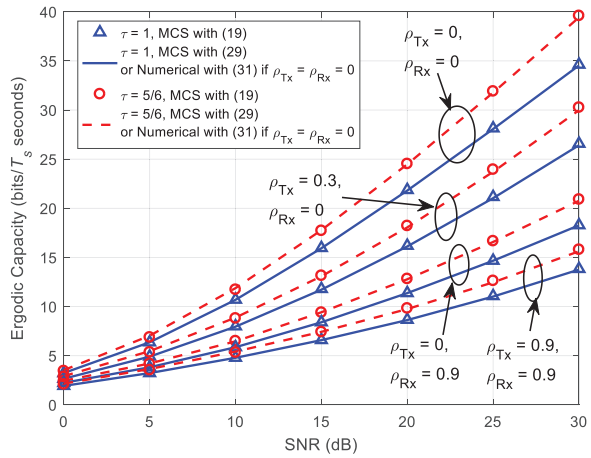

Fig. 6. Ergodic capacity of 4×4 MIMO-FTN system.

and Fig. 8, respectively. When the spatial correlation exists, we only concern the high correlation with $\rho_{\text{Tx}} = \rho_{\text{Rx}} = 0.9$. From Figs. 6∼8, we observe that 1) the MCS results and numerical results agree well; 2) the capacity increases as the SNR increases. At low SNRs, the spatial correlation has little impact on the capacity, as stated in *Remark* 3. For moderate to high SNRs, the capacity growth rate depends on the spatial correlation levels. The lower the spatial correlation is, the larger the growth rate; 3) FTNS also boosts the ergodic capacity in the multi-antenna scenarios; 4) in the MISO and SIMO scenarios, the FTN system with strong spatial correlation has a higher capacity than the Nyquist system without spatial correlation.

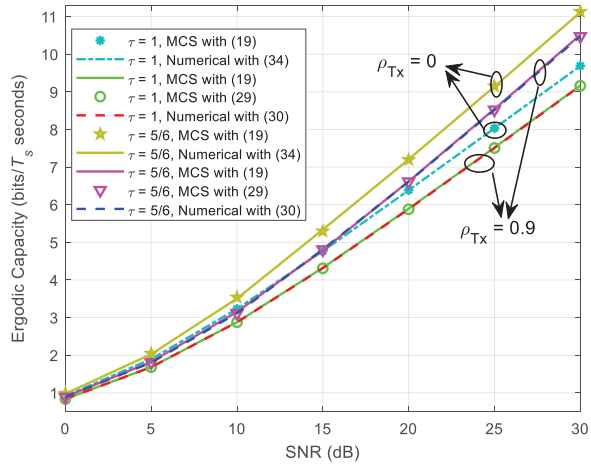

Fig. 7. Ergodic capacity of 4×1 MISO-FTN system.

We now investigate how the FTN gain scales with the

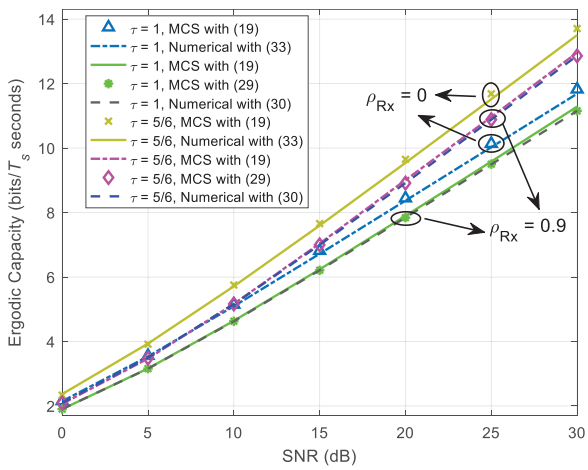

Fig. 8. Ergodic capacity of 1×4 SIMO-FTN system.

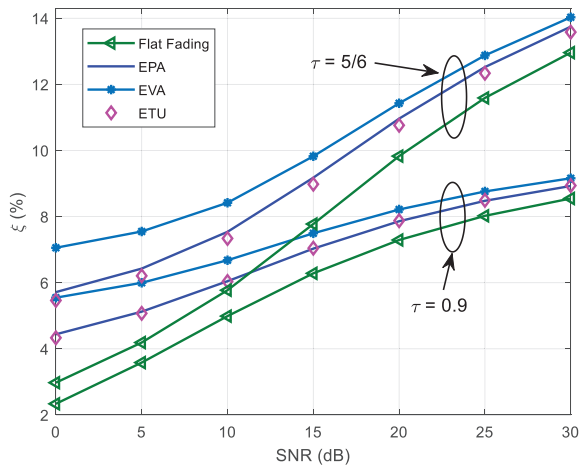

Fig. 9. $\xi\left(0.9, C\left(\alpha\right), 1, 1, \text{SNR}\right)$ and $\xi\left(5/6, C\left(\alpha\right), 1, 1, \text{SNR}\right)$ as a function of SNR for different channel profiles.

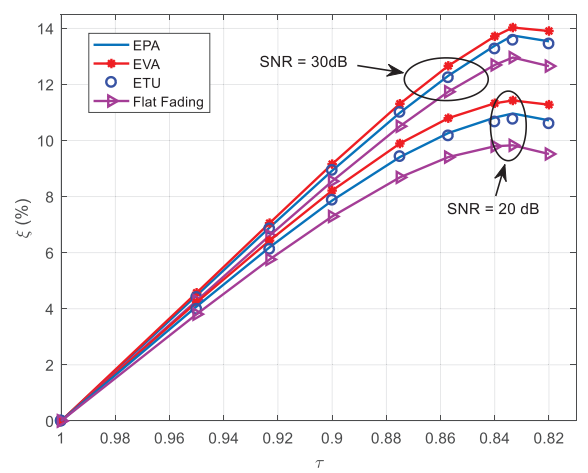

Fig. 10. $\xi\left(\tau, C\left(\alpha\right), 1, 1, 20 \text{ dB}\right)$ and $\xi\left(\tau, C\left(\alpha\right), 1, 1, 30 \text{ dB}\right)$ versus τ for different channel profiles.

frequency and spatial selectivity after seeing the FTN gain and noticing that the time variation has no effect on the ergodic capacity. Let us denote by $\mathcal{C}^{av}_{\text{FTN}}$ and $\mathcal{C}^{av}_{\text{Nyq.}}$ the capacities of FTN and Nyquist systems, respectively. $\mathcal{C}^{av}_{\text{FTN}}$ (or $\mathcal{C}^{av}_{\text{Nyq.}}$) = $\mathcal{C}^{av}_{SISO}$, $\mathcal{C}^{av}_{MIMO}$, $\mathcal{C}^{av}_{SIMO}$, or $\mathcal{C}^{av}_{SIMO}$, depending on the values of M and N. Define $\xi = \left(\mathcal{C}^{av}_{\text{FTN}}/\mathcal{C}^{av}_{\text{Nyq.}} - 1\right) \times 100\%$, the percentage gain yielded by using FTNS over Nyquist signaling. It can be verified that ξ relates with τ, channel PDP $C\left(\alpha\right)$, antenna correlations, and the operating SNR. For clarity, we use $\xi\left(\tau, C\left(\alpha\right), \mathbf{\Psi}_{T_x}, \mathbf{\Psi}_{R_x}, \text{SNR}\right)$ to explicitly denote the dependence.

As mentioned in *Remark* 3, the effects of the frequency selectivity and spatial selectivity on the ergodic capacity are separable. Thus, when analyzing how $\xi\left(\tau, C\left(\alpha\right), \mathbf{\Psi}_{T_x}, \mathbf{\Psi}_{R_x}, \text{SNR}\right)$ varies with frequency selectivity, we consider only SISO channels under which $\mathbf{\Psi}_{T_x} = \mathbf{\Psi}_{R_x} = 1$. Fig. 9 shows $\xi\left(0.9, C\left(\alpha\right), 1, 1, \text{SNR}\right)$ and $\xi\left(5/6, C\left(\alpha\right), 1, 1, \text{SNR}\right)$ versus SNR for different channel profiles, namely the frequency-flat fading, EPA, EVA, and ETU. The maximum delay spreads for EPA, EVA, and ETU are 410 ns, 2510 ns, and 5000 ns, corresponding to the low, medium, and high delay spread environments [36], respectively. For two fixed SNRs, Fig. 10 illustrates the graphs of $\xi\left(\tau, C\left(\alpha\right), 1, 1, 20 \text{ dB}\right)$ and $\xi\left(\tau, C\left(\alpha\right), 1, 1, 30 \text{ dB}\right)$ versus τ. Examining Figs. 9 and 10, we see that

- ξ increases with increasing SNR. For example, let us consider $\tau = 5/6$ and a frequency-flat fading channel. Fig. 9 shows that increasing SNR from 0 dB to 30 dB, ξ increases from 3% to 13%. As SNR approaches infinity, ξ may approach $(1/\tau - 1) \times 100\%$. When assuming an SNR of 200 dB and a frequency-flat fading channel, $\mathcal{C}^{av}_{\text{FTN}} = 72.6592$ bits/T_s seconds and $\mathcal{C}^{av}_{\text{Nyq.}} = 65.6058$ bits/T_s seconds if $\tau = 0.9$, corresponding to $\xi = 10.75\%$. Moreover, $\mathcal{C}^{av}_{\text{FTN}} = 78.0650$ bits/T_s and $\xi = 18.99\%$ if $\tau = 5/6$.
- The FTN gains obtained in the frequency-selective fading channels are higher than those obtained in the frequency-flat fading channels. This can be explained with the plots in Fig. 2. For a given SNR, $\gamma_{\text{SNR}} < 1$ for the Nyquist signaling in the frequency-selective fading channels. Thus, the values of $\mathcal{C}^{av}_{\text{Nyq.}}$ in the frequency-selective fading channels are lower than those in the frequency-flat fading channel. For the FTN case with $\tau = 0.9$ or 5/6, γ_{SNR} almost remains the same under the frequency-selective and flat fading channels. Therefore, the values of $\mathcal{C}^{av}_{\text{FTN}}$ in four channels considered here are close.
- ξ does not scale with respect to the maximum delay spread. The differences among the gains obtained in three frequency-selective fading channels are within 1%.

Now we examine the effects of spatial correlation on ξ. We take the 4×4 MIMO systems with flat fading and EVA channel profiles as examples. Since the spatial correlation has little effect on the ergodic capacity at low SNRs, as we have seen in Figs. 6∼8, we focus on the high-SNR regime, considering an SNR of 30 dB. $\xi\left(\tau, \text{EVA}, \mathbf{\Psi}_{T_x}, \mathbf{\Psi}_{R_x}, 30 \text{ dB}\right)$ and $\xi\left(\tau, \text{Flat Fading}, \mathbf{\Psi}_{T_x}, \mathbf{\Psi}_{R_x}, 30 \text{ dB}\right)$ versus τ for different spatial correlation levels are shown in Fig. 11 and Fig. 12, respectively. Also shown for comparison are $\xi\left(\tau, \text{EVA}, 1, 1, 30 \text{ dB}\right)$ and $\xi\left(\tau, \text{Flat Fading}, 1, 1, 30 \text{ dB}\right)$. It is observed that 1) for MIMO case, the FTN gains are nearly the

same under different correlation levels; 2) the gains obtained in the SISO channel are slightly larger than those in the MIMO channel, and the gain gap grows as τ decreases.

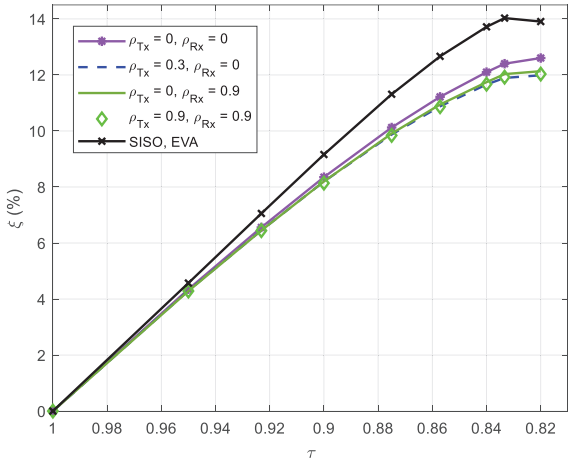

Fig. 11. $\xi\left(\tau, \text{EVA}, \mathbf{\Psi}_{T_x}, \mathbf{\Psi}_{R_x}, 30\text{ dB}\right)$ versus τ for different spatial correlation levels.

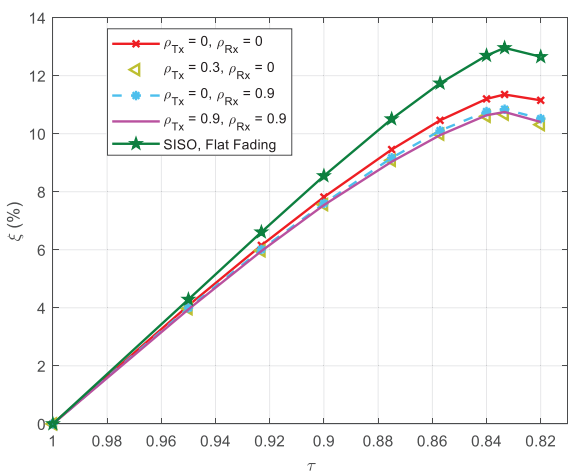

Fig. 12. $\xi\left(\tau, \text{Flat Fading}, \mathbf{\Psi}_{T_x}, \mathbf{\Psi}_{R_x}, 30\text{ dB}\right)$ versus τ for different spatial correlation levels.

V. Conclusion

In this paper, we derive ergodic capacity formulas for the MIMO-FTN transmissions in triply-selective MIMO Rayleigh fading channels and evaluate the capacity under different channel conditions. The ITC resulting from both the frequency-selective channel and the FTNS is taken into account. Furthermore, it is observed that when the FTN-ISI is severe and significantly greater than the channel-induced ISI, the ITC is primarily due to the FTNS. The capacity evaluation reveals that 1) when the RRC filter with $\beta > 0$ is employed, the MIMO-FTN system has a higher capacity than its MIMO-Nyquist counterpart; 2) the channel's time variation has no effect on the ergodic capacity; 3) both the ITC and spatial correlation reduce the ergodic capacity; 4) the FTN gains under different channels are close to the same, while the FTN gain obtained in the frequency-selective fading channel is slightly higher than that obtained in the flat fading channel.

To highlight the value and significance of fundamental limits established in this paper, our future work intends to implement a practical MIMO-FTN system and measure its performance how far away from the limits. Sophisticated algorithms will be developed to close it if the performance gap is significant.

Appendix A
Proof of Proposition 3

It has been shown in [32] that time variations have no influence on ergodic capacity. Thus, as in [34], we prove this proposition by considering slowly time-varying subchannels $c\left(t,\alpha\right)$ that remain constant over K consecutive symbol intervals. Hence, the channel matrix $\mathcal{H}$ becomes a Toeplitz matrix

$$\mathcal{H} = \begin{bmatrix} h\left[k, L_2\right] & \cdots & h\left[k, -L_1\right] & \cdots & 0 \\ \vdots & \ddots & \ddots & \ddots & \vdots \\ 0 & \cdots & h\left[k, L_2\right] & \cdots & h\left[k, -L_1\right] \end{bmatrix}.$$

By using the Szegö's theorem [41] to the product of two Toeplitz matrices $\tilde{\mathbf{R}}_{\mathbf{ZZ}}^{-1/2}$ and $\mathcal{H}$, (19) can be rewritten as

$$\mathcal{C}_{SISO}^{av} = \frac{1}{\tau}\mathbb{E}\left\{\frac{1}{2\pi}\int_0^{2\pi}\log_2\left(1+\tau\gamma\frac{\left|h\left(\omega\right)\right|^2}{g\left(\omega\right)}\right)d\omega\right\}, \quad (36)$$

where $h\left(\omega\right) = \sum_{l=-L_1}^{L_2} h\left[k,l\right]e^{-j\omega l}$ and $g\left(\omega\right) = \sum_k g_\tau\left[k\right]e^{-j\omega k}$. With the three assumptions given in Sec. II-B, it has been shown in Appendix of [33] that the probability density function (PDF) of $\left|h\left(\omega\right)\right|^2$ is equivalent to the PDF of $\left(\lambda\cdot f\left(\omega\right)\right)$ with λ being a unit variance exponentially distributed random variable, and with $f\left(\omega\right)$ being the variance of $h\left(\omega\right)$. Then, we can immediately get (20).

For the inner integral in (20), it equals

$$\begin{aligned}&\frac{1}{2\pi}\int_0^{2\pi}\log_2\left(1+\tau\gamma\lambda\frac{f\left(\omega\right)}{g\left(\omega\right)}\right)d\omega \\ &= \log_2\left(1+\tau\gamma\lambda\frac{f\left(\theta\right)}{g\left(\theta\right)}\right), \theta\in\left[0,2\pi\right)\end{aligned} \quad (37)$$

by using the mean-value theorem of integrals. Define $\tau f\left(\theta\right)/g\left(\theta\right)$ as the SNR degradation factor γ_{SNR}. According to [33], one can approximate γ_{SNR} by fixing λ at its mean value which is 1. Set $\lambda = 1$, (37) becomes

$$\begin{aligned}\frac{1}{2\pi}\int_0^{2\pi}\log_2\left(1+\tau\gamma\frac{f\left(\omega\right)}{g\left(\omega\right)}\right)d\omega &= \log_2\left(1+\gamma\cdot\gamma_{\text{SNR}}\right) \\ &= C_\gamma.\end{aligned} \quad (38)$$

By (38), we can find (23) and (22).

Appendix B
Proof of Corollary 1

In the case of AWGN channel and $p_R\left(t\right) = p_T^*\left(-t\right)$, we have $C\left(\alpha\right) = \delta\left(\alpha\right)$ and $g_{TR}\left(k\tau T_s\right) = g_\tau\left[k\right]$, where $g_\tau\left[k\right]$ is given by (10). Substituting these results into (12) yields

$$c\left[l_1,l_2\right] = g_{TR}\left(l_1\tau T_s\right)g_{TR}^*\left(l_2\tau T_s\right) = g_\tau\left[l_1\right]g_\tau^*\left[l_2\right] \quad (39)$$

It follows that the summation $\sum_{l=-L_1}^{L_2-k} c[l, l+k]$ in (21) equals $\sum_l g_\tau[l] g_\tau^*[l+k]$. Then, $f(\omega) = |g(\omega)|^2$ and C_γ becomes

$$C_\gamma = \frac{1}{2\pi}\int_0^{2\pi} \log_2(1+\tau\cdot\gamma\cdot g(\omega))\, d\omega \tag{40}$$

When $p_R(t)$ is T_s-orthogonal, $g_{\tau=1}[k] = \delta[k]$. Accordingly, $g(\omega) = 1$, $C_\gamma|_{\tau=1} = \log_2(1+\gamma)$ and $\gamma_{\text{SNR}}|_{\tau=1} = 1$.

It has been shown in [1, eq. (3.15)] that

$$\begin{aligned} g(\omega) &= \frac{1}{\tau T_s}\sum\nolimits_k \left| P_R\left(\frac{\omega}{2\pi\tau T_s} + \frac{k}{\tau T_s}\right)\right|^2 \\ &= \frac{1}{\tau T_s} P_R^{\text{fo}}\left(\frac{\omega}{2\pi\tau T_s}\right). \end{aligned} \tag{41}$$

Upon substituting for $g(\omega)$ from (41) and recalling that $\gamma = PT_s/N\sigma_\upsilon^2$, we have

$$\begin{aligned} C_\gamma &= \frac{1}{2\pi}\int_{-\pi}^{\pi} \log_2\left(1+\frac{P}{N\sigma_\upsilon^2}P_R^{\text{fo}}\left(\frac{\omega}{2\pi\tau T_s}\right)\right) d\omega \\ &= 2\tau T_s\int_0^{1/2\tau T_s} \log_2\left(1+\frac{P}{N\sigma_\upsilon^2}P_R^{\text{fo}}(f)\right) df. \end{aligned} \tag{42}$$

By noting that the channel gain is deterministic and $|h(\omega)|^2 = |g(\omega)|^2$ in the AWGN channel, we can drop the expectation operation in (36) and obtain

$$\mathcal{C}_{SISO}^{av} = C_\gamma/\tau \text{ bits}/T_s \text{ seconds}. \tag{43}$$

Dividing both sides by T_s gives (26).

We now prove inequality (27). As $p_R(t)$ is T_s-orthogonal, $\sum_k \left|P_R\left(f+\frac{k}{T_s}\right)\right|^2 = T_s, |f| \leqslant 1/2T_s$ and $P_R^{\text{fo}}(f) \leqslant T_s$ if $\tau < 1$, which result in

$$\begin{aligned} C_\gamma &= 2\tau T_s\int_0^{1/2\tau T_s} \log_2\left(1+\frac{P}{N\sigma_\upsilon^2}P_R^{\text{fo}}(f)\right) df \\ &\leqslant \log_2\left(1+\frac{PT_s}{N\sigma_\upsilon^2}\right) = \log_2(1+\gamma). \end{aligned} \tag{44}$$

Using (23), (27) can be directly obtained.

Appendix C
Proof of Proposition 4 and Corollary 3

Again we consider the slowly time-varying channels. Now the channel matrix $\mathcal{H}$ is a block Toeplitz matrix

$$\mathcal{H} = \begin{bmatrix} \mathbf{H}_{L_2}[k] & \cdots & \mathbf{H}_{-L_1}[k] & \cdots & \mathbf{0} \\ \vdots & \ddots & \ddots & \ddots & \vdots \\ \mathbf{0} & \cdots & \mathbf{H}_{L_2}[k] & \cdots & \mathbf{H}_{-L_1}[k] \end{bmatrix}.$$

Similar to (36), we can use the Szegö's theorem and obtain

$$\begin{aligned} \mathcal{C}_{MIMO}^{av} = \frac{1}{\tau}\mathbb{E}_{\mathcal{H}}\Bigg\{\frac{1}{2\pi}\int_0^{2\pi} \log_2\det(\mathbf{I}_M + \\ \tau\gamma\frac{\mathbf{H}(\omega)\mathbf{H}^{\text{H}}(\omega)}{g(\omega)}\Bigg) d\omega\Bigg\} \end{aligned} \tag{45}$$

where the $M\times M$ matrix $\mathbf{H}(\omega)$ is defined as

$$\mathbf{H}(\omega) = \sum\nolimits_{l=-L_1}^{L_2} \mathbf{H}_l[k] e^{-jl\omega}. \tag{46}$$

With the three assumptions given in Sec. II-B, it has been shown in [34, Appendix B] that the statistical properties of $\mathbf{H}(\omega)\mathbf{H}^{\text{H}}(\omega)$ are identical to those of the product matrix $f(\omega)\cdot\mathbf{\Psi}_{R_x}\mathbf{H}_W\mathbf{\Psi}_{T_x}\mathbf{H}_W^{\text{H}}$, where $f(\omega)$ is given by (21) and $\mathbf{H}_W$ is an $M\times N$ matrix with all elements being i.i.d. ZMCSCG random variables. Moreover, using the mean-value theorem of integrals to (45), we obtain

$$\begin{aligned} \mathcal{C}_{MIMO}^{av} &= \frac{1}{\tau}\mathbb{E}_{\mathbf{H}_W}\Bigg\{\frac{1}{2\pi}\int_0^{2\pi} \log_2\det(\mathbf{I}_M + \\ &\qquad \tau\gamma f(\omega)\frac{\mathbf{\Psi}_{R_x}\mathbf{H}_W\mathbf{\Psi}_{T_x}\mathbf{H}_W^{\text{H}}}{g(\omega)}\Bigg)\Bigg\} \\ &= \frac{1}{\tau}\mathbb{E}_{\mathbf{H}_W}\{\log_2\det(\mathbf{I}_M + \\ &\qquad \left(2^{C_\gamma}-1\right)\mathbf{\Psi}_{R_x}\mathbf{H}_W\mathbf{\Psi}_{T_x}\mathbf{H}_W^{\text{H}})\}. \end{aligned} \tag{47}$$

This completes the proof of proposition 4.

When $\mathbf{\Psi}_{T_x}$ and $\mathbf{\Psi}_{R_x}$ both are identity matrices, the distribution of $\mathbf{H}(\omega)\mathbf{H}^{\text{H}}(\omega)$ is the same as the distribution of $f(\omega)\cdot\mathbf{H}_W\cdot\mathbf{H}_W^{\text{H}}$. As $\mathbf{H}_W\mathbf{H}_W^{\text{H}}$ is a Wishart matrix, we obtain (48) by invoking theorem 2 of [40].

$$\begin{aligned} \mathcal{C}_{MIMO}^{av} &= \frac{1}{\tau}\mathbb{E}_{\mathbf{H}_W}\left\{\log_2\det\left(\mathbf{I}_M + \left(2^{C_\gamma}-1\right)\mathbf{H}_W\mathbf{H}_W^{\text{H}}\right)\right\} \\ &= \frac{1}{\tau}\int_0^\infty \log_2\left(1+\left(2^{C_\gamma}-1\right)\lambda\right) V(\lambda)\, d\lambda. \end{aligned} \tag{48}$$

This completes the proof of corollary 3.

References

[1] F. Rusek, "Partial response and faster-than-Nyquist signaling," Ph.D. dissertation, Dept. Elec. Inform. Tech., Lund Univ., Lund, Sweden, Sep. 2007.

[2] J. B. Anderson, F. Rusek *et al.*, "Faster-than-Nyquist signaling," *Proc. IEEE*, vol. 101, no. 8, pp. 1817–1830, Aug. 2013.

[3] A. Modenini, F. Rusek, and G. Colavolpe, "Faster-than-Nyquist signaling for next generation communication architectures," in *Proc. 22nd Eur. Signal Process. Conf. (EUSIPCO)*, Lisbon, Portugal, Sep. 2014, pp. 1856–1860.

[4] C. Le, M. Schellmann *et al.*, "On the practical benefits of faster-than-Nyquist signaling," in *Proc. Int Conf. on Advanced Tech. Commun. (ATC)*, Hanoi, Vietnam, Oct. 2014, pp. 208–213.

[5] "From today to tomorrow: Huawei microwave & mm-wave whitepaper," Huawei, Shenzhen, China, Tech. Rep., 2016. [Online]. Available: https://www-file.huawei.com/-/media/CORPORATE/PDF/white%20paper/huawei-microwave-whitepaper-2016.pdf

[6] J. Fan, S. Guo *et al.*, "Faster-than-Nyquist signaling: an overview," *IEEE Access*, vol. 5, pp. 1925–1940, Feb. 2017.

[7] M. Maso and S. Tomasin, "Pre-equalized faster than Nyquist transmission for 5G cellular microwave backhaul," in *Proc. IEEE Int. Workshop Signal Process. Advances Wireless Commun. (SPAWC)*, Edinburgh, UK, July 2016, pp. 1–6.

[8] T. Ishihara, S. Sugiura *et al.*, "The evolution of faster-than-Nyquist signaling," *IEEE Access*, vol. 9, pp. 86 535–86 564, June 2021.

[9] W. Yuan, N. Wu *et al.*, "Iterative joint channel estimation, user activity tracking, and data detection for FTN-NOMA systems supporting random access," *IEEE Trans. Commun.*, vol. 68, no. 5, pp. 2963–2977, May 2020.

[10] S. Li, Z. Wei *et al.*, "Faster-than-Nyquist asynchronous NOMA outperforms synchronous NOMA," *IEEE J. Select. Areas Commun.*, vol. 40, no. 4, pp. 1128–1145, April 2022.

[11] M. Jana, L. Lampe *et al.*, "Dual-polarized faster-than-Nyquist transmission using higher order modulation schemes," *IEEE Trans. Commun.*, vol. 66, no. 11, pp. 5332–5345, Nov. 2018.

[12] S. C. D. Spano, M. Alodeh and B. Ottersten, "Faster-than-Nyquist signaling through spatio-temporal symbol-level precoding for the multiuser MISO downlink channel," *IEEE Trans. Wireless Commun.*, vol. 17, no. 9, pp. 5915–5928, Sep. 2018.

[13] F. Rusek and J. B. Anderson, "Constrained capacities for faster-than-Nyquist signaling," *IEEE Trans. Inform. Theory*, vol. 55, no. 2, pp. 764–775, Feb. 2009.

[14] Y. J. D. Kim, "Properties of faster-than-Nyquist channel matrices and folded-spectrum, and their applications," in *Proc. IEEE Wireless Commun. Networking Conf.*, Doha, Qatar, Apr. 2016, pp. 1–7.

[15] Y. J. D. Kim and J. Bajcsy, "Information rates of cyclostationary faster-than-Nyquist signaling," in *Proc. 12th Canadian Workshop Info. Theory*, Kelowna, Canada, May 2011, pp. 1–4.

[16] D. Kapetanovic and F. Rusek, "The effect of signaling rate on information rate for single carrier linear transmission systems," *IEEE Trans. Commun.*, vol. 60, no. 2, pp. 421–428, Feb. 2012.

[17] M. Ganji, X. Zou, and H. Jafarkhani, "On the capacity of faster than Nyquist signaling," *IEEE Commun. Lett.*, vol. 24, no. 6, pp. 1197–1201, June 2020.

[18] T. Ishihara and S. Sugiura, "SVD-precoded faster-than-Nyquist signaling with optimal and truncated power allocation," *IEEE Trans. Wireless Commun.*, vol. 18, no. 12, pp. 5909–5923, Dec. 2019.

[19] J. T. Wang, "Performance analysis for faster-than-Nyquist signaling under multi-path channel," *IEEE Commun. Lett.*, vol. 24, no. 2, pp. 302–306, Feb. 2020.

[20] ——, "Faster-than-Nyquist signaling with time-based receive transformation," *Wireless Personal Commun.*, vol. 108, pp. 2445–2454, June 2021.

[21] T. Ishihara and S. Sugiura, "Eigendecomposition-precoded faster-than-Nyquist signaling with optimal power allocation in frequency-selective fading channels," *IEEE Trans. Wireless Commun.*, vol. 21, no. 3, pp. 1681–1693, March 2022.

[22] M. Yuhas, Y. Feng, and J. Bajcsy, "On the capacity of faster-than-Nyquist MIMO transmission with CSI at the receiver," in *Proc. IEEE Globecom Workshops (GC Wkshps)*, San Diego, USA, Dec. 2015, pp. 1–6.

[23] J. T. Wang, "Time-space MIMO system with faster-than-Nyquist signaling in frequency-selective fading channel," *Multidim. Syst. Signal Process.*, vol. 32, pp. 1027–1039, July 2021.

[24] J. P. Kermoal, L. Schumacher *et al.*, "A stochastic MIMO radio channel model with experimental validation," *IEEE J. Sel. Areas Commun.*, vol. 20, no. 6, pp. 1211–1226, Aug. 2002.

[25] X. Gao, O. Edfors *et al.*, "Massive MIMO performance evaluation based on measured propagation data," *IEEE Trans. Wireless Commun.*, vol. 14, no. 7, pp. 3899–3911, July 2015.

[26] R. B. Ertel *et al.*, "Overview of spatial channel models for antenna array communication systems," *IEEE Personal Commun.*, vol. 5, no. 1, pp. 10–22, Feb. 1998.

[27] W. Yuan, N. Wu, H. Wang *et al.*, "Variational inference-based frequency-domain equalization for faster-than-Nyquist signaling in doubly selective channels," *IEEE Signal Process. Lett.*, vol. 23, no. 9, pp. 1270–1274, Sept. 2016.

[28] N. Wu, W. Yuan, H. Wang *et al.*, "Frequency-domain iterative message passing receiver for faster-than-Nyquist signaling in doubly selective channels," *IEEE Wireless Commun. Lett.*, vol. 5, no. 6, pp. 584–587, Dec. 2016.

[29] Q. Shi, N. Wu, X. Ma *et al.*, "Frequency-domain joint channel estimation and decoding for faster-than-Nyquist signaling," *IEEE Trans. Commun.*, vol. 66, no. 2, pp. 781–795, Feb. 2018.

[30] C. Sgraja and C. Xiao, "On discrete-time modeling of time-varying WSSUS fading channels," in *Proc. IEEE Int. Conf. Commun.*, Istanbul, Turkey, June 2006, pp. 5486–5490.

[31] C. Xiao, J. Wu *et al.*, "A discrete-time model for triply selective MIMO Rayleigh fading channels," *IEEE Trans. Wireless Commun.*, vol. 3, no. 5, pp. 1678–1688, Sept. 2004.

[32] C. Xiao and Y. R. Zheng, "Ergodic capacity, capacity distribution and outage capacity of MIMO time-varying and frequency-selective Rayleigh fading channels," in *Proc. 41st Annual Allerton Conf. Commun. Control and Computing.*, Illinois, USA, Oct. 2003, pp. 346–355.

[33] ——, "Ergodic capacity of doubly selective Rayleigh fading MIMO channels," in *Proc. IEEE Wireless Commun. Networking Conf.*, Atlanta, USA, Mar 2004, pp. 345–350.

[34] ——, "On the ergodic capacity of MIMO triply selective Rayleigh fading channels," *IEEE Trans. Wireless Commun.*, vol. 7, no. 6, pp. 2272–2279, June 2008.

[35] S. Barbarossa, *Multiantenna wireless communications systems*. MA, USA: Artech House, 2005.

[36] H. Zarrinkoub, *Understanding LTE with MATLAB: From mathematical foundation to simulation, performance evaluation and implementation*. Chichester, West Sussex, UK: Wiley, 2014.

[37] D. S. Shiu, G. J. Foschini *et al.*, "Fading correlation and its effect on the capacity of multielement antenna systems," *IEEE Trans. Commun.*, vol. 48, no. 3, pp. 502–513, Mar. 2000.

[38] C.-N. Chuah, D. Tse, J. Kahn, and R. Valenzuela, "Capacity scaling in MIMO wireless systems under correlated fading," *IEEE Trans. Inform. Theory*, vol. 48, no. 3, pp. 637–650, Mar. 2002.

[39] ETSI, "Universal Mobile Telecommunications System (UMTS); Selection procedures for the choice of radio transmission technologies of the UMTS," TR 101 112 (V3.2.0), Mar. 1998. [Online]. Available: https://portal.3gpp.org/desktopmodules/Specifications/SpecificationDetails.aspx?specificationId=1782

[40] E. Telatar, "Capacity of multi-antenna Gaussian channels," *Eur. Trans. Telecommun.*, vol. 10, no. 6, pp. 585–595, Nov. 1999.

[41] R. M. Gray, *Toeplitz and Circulant Matrices: A Review*. The Netherlands: Now Publishers, 2006.